Cardiovascular Engineering and Technology, Vol. 10, No. 4, December 2019 *(© 2019)* pp. 648–659
https://doi.org/10.1007/s13239-019-00430-5

Embolus Transport Simulations with Fully Resolved Particle Surfaces

PATRICK M. MCGAH

Siemens PLM Software Inc., 13810 SE Eastgate Way, Bellevue, WA 98005, USA

(Received 12 April 2019; accepted 28 August 2019; published online 16 September 2019)

Associate Editors David Steinman and Ajit P. Yoganathan oversaw the review of this article.

Abstract

Purpose—There has been interest in recent work in using computational fluid dynamics with Lagrangian analysis to calculate the trajectory of emboli-like particles in the vasculature. While previous studies have provided an understanding of the hemodynamic factors determining the fates of such particles and their relationship to risk of stroke, most analyses have relied on a particle equation of motion that assumes the particle is "small" e.g., much less than the diameter of the vessel. This work quantifies the limit when a particle can no longer be considered "small".

Methods—The motion of embolus-like particles are simulated using an overset mesh technique. This allows the fluid stresses on the particle surface to be fully resolved. Consequently, the particles can be of arbitrary size or shape. The trajectory of resolved particles and "small" particles are simulated through a patient-specific carotid artery bifurcation model with particles 500, 1000, and 2000 μm in diameter. The proportions of particles entering the internal carotid artery are treated as the outcome of the particle fate, and statistical comparisons are made to ascertain the importance of non-small particle effects.

Results—For the 2000 μm embolus, the proportion of particles traveling to the internal carotid artery is $74.7 \pm 1.3\%$ (mean $\pm$ 95% confidence margin) for the "small" particle model and is $85.7 \pm 5.4\%$ for a resolved particle model. The difference is statistically significant, $p < 0.05$, based on the binomial test for the particle outcomes. No statistically discernible differences are found for the smaller diameter particles.

Conclusions—Quantitative differences are observable for the 2000 μm trajectories between the "small" and resolved particle models which is a particle diameter 27% relative to the common carotid artery diameter. A fully resolved particle model ought to be considered for emboli trajectory simulations when the particle size ratio is $\gtrsim$ 20%.

Address correspondence to Patrick M. McGah, Siemens PLM Software Inc., 13810 SE Eastgate Way, Bellevue, WA 98005, USA. Electronic mail: patrick.mcgah@siemens.com

INTRODUCTION

About 800,000 people per year in the United States experience a stroke, with approximately 87% of these strokes being ischemic in cause.[6] Embolic strokes, whereby an embolus originating from either the heart, the proximal cerebral arteries or the aortic arch, or from the veins (paradoxical embolism), are estimated to be between 15 and 30% of all cases of ischemic stroke.[3] Embolic strokes result in higher in-hospital mortality than other types of ischemic stroke like atherosclerotic or lacunar due to the fact that a larger portion of the cerebral tissue tends to be affected.

While it is evident that the trajectory of an embolus is highly influenced by hemodynamic forces, non-intuitive results have been found in previous studies. *In vitro* experiments by Bushi *et al.*[7] found that smaller particles tended to travel into the daughter vessel of idealized y-shaped bifurcations in a proportion expected by the distribution of the Eulerian volumetric flow rate. Surprisingly, larger particles tended to preferentially travel into the larger vessels at a proportion greater than what would be expected by the volumetric flow rate alone. Similarly, Chung *et al.*[9] also conducted *in vitro* investigations of particle trajectories in a patient-specific model of the circle of Willis. They found that larger (1 mm) particles entered the middle cerebral arteries, the largest of the cerebral arteries, at a rate disproportionately higher than the volumetric flow rate. These findings suggest that the particle inertia is important in determining its trajectory.

Subsequently, there is interest in using computational fluid dynamics (CFD) with Lagrangian particle analysis to calculate trajectories of emboli. These techniques could be used, for example, in pre-surgical planning and stroke risk assessment for medical de-

1869-408X/19/1200-0648/0 © 2019 Biomedical Engineering Society

vices such as left ventricular assist devices[2]; cerebrovascular events are a major cause of morbidity and mortality in patients with ventricular assist devices.

Carr[8] used CFD with Lagrangian analysis to track the trajectories of cardiogenic emboli through patient-specific models of the aorta and branch arteries to the head. They found that a particle's size strongly predicted the probability that a particle travels to the vertebral and carotid arteries vs. to the descending aorta. They found that particles $\approx$ 1 mm in diameter were found to travel to the superior circulation at a proportion twice that of the volumetric flow rate distribution. Conversely, they found that smaller particles ($\lesssim$0.25 mm diameter) traveled to the superior circulation at a rate nearly equal to the volumetric flow rate distribution. This supports the notion that the inertia of the smaller particles is not important and that the particles travel like flow tracers.

Fabbri[10] studied the trajectories of emboli through the basilar artery, carotid artery, and the circle of Willis using CFD and Lagrangian analysis. Their results are again consistent with the *in vitro* observation that larger sized particles ($>$ 0.5 mm) released into the carotid arteries travel into the larger middle cerebral artery at a rate higher than that of the volumetric flow distribution. They also found that all particles released into the basilar artery only traversed into the posterior cerebral circulation.

In any Lagrangian fluid dynamics analysis, an equation of motion, which relates the hydrodynamic forces on the particle to its temporal acceleration, must be specified. In previous computational studies of emboli transport, the Maxey–Riley equation[17] (or some modification thereof) is used as the basis for the particle equation of motion. Maxey–Riley is a complete theoretical description derived from first principles. The equation contains contributions from the added mass force, the background flow pressure gradient and shear forces, the Stokes drag force, buoyancy force, and the Basset history force.

Despite the completeness of Maxey–Riley equation, it does make several simplifying assumptions in its derivation. Most importantly, it assumes that: (1) the particle is "small" (discussed in more depth below), (2) the particle Reynolds number is small i.e., $Re_p \ll 1$, (3) the particle is not influenced by walls, boundaries, or other particles in the domain. The Maxey–Riley equation may be modified, albeit usually in *ad hoc* manner, to correct for some of these assumptions. The second assumption can be corrected by modifying the expression for the forces. Specifically, the drag force can be corrected by modifying the particle drag coefficient at finite Reynolds numbers with a semi-empirical formula.[18] Several previous studies[10,19] used a particle equation accounting for finite Re_p in the drag force. Interestingly, the added mass force does not require a correction at finite Re_p. The third assumption is not typically modified for typical analyses, though the Stokes drag force is known to be modified even for a small a particle when it is near a solid boundary. For the purposes of modeling the trajectory of emboli in the arteries, the first assumption, however, is likely the most restrictive.

The first assumption requires that the particle is small compared to the length scale of the flow e.g., $d \ll L$ where d is the particle diameter and L is the flow length scale. For arterial flows, the parent vessel diameter, D, is usually the relevant flow length scale. Several terms in Maxey–Riley explicitly require the particle to be small. For example, the force due to the pressure differences in the undisturbed background flow is calculated by evaluating the pressure gradient at the position of the particle. This assumption is only valid if the pressure gradient is constant over the surface of the particle which requires that the particle is small. Furthermore, the functional form of the drag coefficient is likely not formally correct for large particles even when accounting for finite Re_p effects.

Previously mentioned studies have provided important fluid mechanical insights into the factors determining the fate of emboli. Importantly, they have confirmed findings of *in vitro* experiments and have justified the utility of Lagrangian-based CFD analyses for emboli transport. However, they have applied their analysis to relatively large particles, up to or even above 50% diameter ratios. Carr[8] analyzed emboli 4 mm in diameter in models with common carotid artery diameters $\approx$ 8 mm, while Fabbri[10] analyzed emboli 1 mm in diameter in a model of cerebral vessels 1–4 mm in diameter. These studies did candidly acknowledge the limitation of using larger sized particles in conjunction with the Maxey–Riley equation. However, it is not known to what degree a Lagrangian analysis utilizing a "small particle assumption" is reliable when applied to larger particles.

A study from Mukherjee *et al.*[20] compared emobli trajectories from one-way and two-way coupled simulations; two-way coupling allows a particle's momentum to feed back into, and subsequently modify, the Eulerian flow field. They found that the inclusion of two-way coupling effects is relatively unimportant for embolus diameters up to $\approx$ 20% of the parent vessel diameter. However, the two-way coupling approach is fundamentally a "small" particle model as the particle equation of motion is a modified version of the Maxey–Riley equation.

The limitation of the small particle assumption has clinical relevance as emboli may be up to several millimeters in size. For instance, in patients undergoing coronary artery bypass grafting, emboli of 0.3–2.9 mm in diameter were detected by Barbut *et al.*[5] using transesophageal echocardiography. Similarly, Reichenspurner *et al.*[22] also detected emboli of 0.1–6 mm in diameter which were captured by an intra-aortic filter temporarily inserted in patients undergoing coronary artery bypass grafting. Lastly, the sizes of left atrial thrombi, the most common source of cardiogenic emboli,[3] have been measured by Manning *et al.*[16] after surgical removal to be up to several centimeters in size.

This study aims to help answer at what point the small particle assumption is no longer reliable in the analysis of emboli transport. We utilize an overset mesh technique, in conjunction with a six degrees of freedom (6DOF) rigid body solver, to simulate the motion of emboli-like particles. The technique fully resolves the flow field near the particle surface and the fluid stresses on the particle surface. Consequently, the method can simulate particles of arbitrary size and arbitrary shape. Furthermore, the overset approach is also inherently two-way coupled as the translation or rotation of the rigid body can induce fluid velocities which feedback into the Eulerian flow solution.

Several existing studies have investigated the trajectory of emboli using methods that fully resolve the particle's surface. Aycock *et al.*[4] used an immersed boundary method to calculate the trajectories of rigid emboli in order to determine the capture efficiency of vena cava filters. Additionally, arbitrary Lagrangian-Eulerian (ALE) formulations with mesh deformation and automatic mesh coarsening/refining have also been used to study emboli trajectories for rigid[23] and deformable[1] emboli. These studies have importantly shown the feasibility and utility of non-small emboli transport simulations. However, no study to date has undertaken a systematic investigation to determine under what conditions a resolved particle model produces quantitatively different results than a "small" particle model.

We simulate the trajectory of an ensemble of particles through the carotid artery bifurcation using both the overset technique and a small particle assumption equation of motion in order to discern statistical differences in the trajectories calculated by the two methods. Our hypothesis is that *the resolved and "small" particle trajectories will be consistent when the size of the resolved particle is sufficiently small, but the trajectories will show discernible differences if the resolved particle becomes large enough.*

METHODS

3D Vascular Anatomy

The carotid artery bifurcation is studied in this work as a representative example of the vasculature. A 3D reconstruction of a non-atherosclerotic carotid bifurcation is obtained from 3D ultrasound examination of a single subject during a previous study.[27] A closely spaced stack of 2D images is acquired by gray-scale (B-mode) images of the carotid artery. The 3D surface model is generated from the segmented lumen of the 2D images.

For reference, the diameters of the common carotid artery (CCA), internal carotid artery (ICA), and external carotid artery (ECA) are 7.3, 5.9, and 5.3 mm, respectively. An image of the vessel surface reconstruction is shown in Fig. 1.

Eulerian Flow Model

The Eulerian flow field of the blood is simulated using the code Simcenter STAR-CCM+ v. 12.06 (Siemens PLM Software Inc.), a finite-volume based code for solving the incompressible Navier–Stokes equations. The flow is solved with an unstructured polyhedral mesh with a nominal cell size of 0.175 mm, resulting in a total mesh count of about 1.0 million cells. The solution is integrated in time with a 2nd order BDF scheme using a time step size of 0.25 ms. The blood is treated as a Newtonian fluid with viscosity $\mu = 3.5$ cP and density $\rho_f = 1050$ kg/m^3.

For the CCA boundary conditions, a Womersley flow velocity profile is prescribed with a mean and max flow rate of 477 and 1520 mL/min, respectively. The shape of the waveform is taken from Holdsworth *et al.*[14] who measured the CCA volume flow rates with Doppler ultrasound. The Womersley number and mean Reynolds number of the CCA are 5.45 and 415, respectively.

For the ICA and ECA boundary conditions, the pressure is prescribed by three-element Windkessel models.[26] For the ICA, the model parameters are: $R = 2.098 \times 10^9\ \mathrm{kg\,m^{-4}\,s^{-1}}$, $Z = 5.24 \times 10^8\ \mathrm{kg\,m^{-4}\,s^{-1}}$, and $C = 4.766 \times 10^{-10}\ \mathrm{m^4\,s^2\,kg^{-1}}$. The parameters for the ECA are: $R = 2.86 \times 10^9\ \mathrm{kg\,m^{-4}\,s^{-1}}$,

FIGURE 1. Reconstructed carotid bifurcation anatomy used for all simulations in this work.

$Z = 7.14 \times 10^8\,\mathrm{kg\,m^{-4}\,s^{-1}}$, and $C = 3.506 \times 10^{-10}\,\mathrm{m^4\,s^2\,kg^{-1}}$. This results in a mean flow split between the ICA and ECA of 57.7 and 42.3%.

Particle Injection and Initialization

After the Eulerian flow filed has progressed for three cardiac cycles, either "small" or "non-small" (i.e., resolved) particles are injected at the CCA, depending on the respective simulation. The emboli are treated as spherical particles with diameters of 500 μm, 1000 μm, and 2000 μm, resulting in size ratios of 6.8, 13.7, and 27.3%, respectively, compared to the CCA diameter. The particle is assumed to be slightly heavier than the blood with a density $\rho_p = 1100\ \mathrm{kg/m^3}$ ($\rho_p/\rho_f \approx 1.05$). The "small" and resolved particle trajectories are also computed using Simcenter STAR-CCM+.

The initial position of each particle's centroid is specified by sampling an assumed *uniform probability density function* across the inlet face of the CCA. The outer edge of the initial position distribution is slightly smaller than the CCA diameter in order to prevent a particle's surface from overlapping with the lumen. Particles are injected at temporal increments of 1/20 the cardiac cycle for one cardiac cycle. The simulation is advanced in time until the particle touches the outflow boundary of the either the ICA or ECA. A particle's initial velocity is set to be equal to that of the same Eulerian mesh cell where the particle is injected into the domain.

The "small" particles are simulated by one-way coupling analysis whereby the Eulerian flow influences a particle's dynamics, but the flow disturbance created by the particle does not feedback into the Eulerian flow field. Thus "small" particle trajectories do not influence one another. Many small particle trajectories may be simulated at the same time in a given simulation. The resolved particle simulations, on the other hand, are inherently two-way coupled. As a result, each resolved particle simulation consists of only a single particle so that particles are not artificially influenced by possible interactions with one another. For each particle size, about 5000 "small" particle trajectories are calculated, while about 50 are calculated for each resolved particle size.

Particle Trajectory Statistical Analysis

Given that the initial conditions of each particle are spatially randomized, and that the particles are injected at differing points in the cardiac cycle, one can then consider the trajectory of each particle to be a realization of some statistical event. There are two possible statistical outcomes for a particle: traveling either to the ICA or the ECA. Therefore, the probability that a particle travels into the ICA will follow a binomial distribution.

The binomial distribution can be used to estimate the confidence intervals for the probability that a particle will enter the ICA as a function of particle size or particle model (i.e., "small" vs. resolved) by considering the completed set of all particle trajectories. Furthermore, the binomial test can be used to determine if the outcome probabilities for "small" particles are different in a statistically meaningful way from those of resolved particles. As stated in Section "Introduction", our hypothesis is that the outcome probabilities for "small" and resolved particles will be nearly equal when the resolved particle size is sufficiently small, but that the probabilities will be different if the resolved particle size is large.

For large sample sizes, the binomial distribution can be approximated by a normal distribution. All statistical results reported herein will utilize the normal approximation for the binomial distribution.

Small Particle Model

Particles modeled using the "small" assumption have three translational but no rotational degrees of freedom. The trajectories of the "small" particles are governed by a modified form of the Maxey–Riley equation, namely:

$$\rho_p V_p \frac{d\mathbf{v}}{dt} = \rho_f V_p \frac{D\mathbf{u}}{Dt} + \frac{1}{2}\rho_f V_p \left(\frac{D\mathbf{u}}{Dt} - \frac{d\mathbf{v}}{dt}\right) - \frac{1}{2} C_D\, \rho_f\, A_p |\mathbf{v} - \mathbf{u}|(\mathbf{v} - \mathbf{u}) \tag{1}$$

where V_p is the particle volume, C_D is the particle drag coefficient, A_p is the particle cross-sectional area, $\mathbf{v}$ is the particle velocity, and $\mathbf{u}$ is the undisturbed flow velocity evaluated at the centroid of the particle. The forces on the right-hand side of the equation represent: the background flow net pressure and viscous forces, the added mass force, and the quasi-steady drag force, respectively. The Basset history force is neglected here; it is rarely included in the equation of motion because of its computational difficulty[25] rather than because of physical considerations. The Schiller–Naumann correlation is used to specify the the drag coefficient as a function of the particle Reynolds number:

$$C_D = \begin{cases} \frac{24}{Re_p}(1 + 0.15 \cdot Re_p^{0.687}) & Re_p \le 10^3 \\ 0.44 & Re_p > 10^3 \end{cases} \tag{2}$$

where Re_p is the Reynolds number based on the particle diameter, d, and slip velocity, i.e., $\rho_f|\mathbf{v} - \mathbf{u}|d/\mu$. It

should be noted, however, that Re_p was not found to exceed 10^3 in the simulations below.

Inertialess tracer particles are injected into the domain. The tracer results are reported as "zero diameter" particles in the results below. Both the inertial and inertialess particle equations are integrated by an explicit Euler method with automatic time step control; the time step is chosen so that the Courant number based on the particle speed and local mesh size is less than 0.35.

Wall Collision Model

Particle interactions with walls are treated as frictionless, perfectly elastic collisions (i.e., coefficient of restitution is 1 in both the normal and tangential directions). The particle velocity component tangential to a wall is unchanged in a collision, and the component normal to a wall is recalculated as its negative after a collision. The collision model implicitly assumes that the particle rebound happens instantaneously.

Resolved Particle Model

The non-small, or resolved, particle motion is computed based on an overset mesh, also called a Chimera mesh, approach. The technique allows the flow in the near-field of the particle and the fluid stresses on the particle to be fully resolved. The technique in STAR-CCM+ is largely based on the work of Hadžić.[11]

Fundamentally, the approach has two meshes that can overlap each other in an arbitrary manner. First is the background mesh, which encompasses the entire solution domain and is equivalent to a standard CFD mesh. Second is the overset mesh which surrounds only the embolus. The overset mesh is "set over" the background mesh. The mesh cells in the background mesh that are "beneath" the overset mesh are deactivated and no equations are solved in them; however, the deactivated cells can become reactivated and active cells can become deactivated as the overset mesh moves through the domain. The solution fields between the two meshes are implicitly coupled. Field values in "donor cells" at the edge of the active cells region in each mesh are coupled to their nearest "acceptor cells" on the opposing side of the respective partner mesh. The respective donor cells of a given acceptor cell are found by linear interpolation using shape functions spanning a tetrahedron defined by the centroids of the donor cells.

The embolus itself is treated as spherical 6DOF rigid body which obeys the Newton–Euler equations for linear and angular momentum. The governing equations are:

$$\rho_p V_p \frac{d\mathbf{v}}{dt} = \mathbf{F} \tag{3}$$

$$\mathbf{I}\frac{d\boldsymbol{\omega}}{dt} + \boldsymbol{\omega} \times \mathbf{I}\boldsymbol{\omega} = \mathbf{M} \tag{4}$$

where $\mathbf{F}$ and $\mathbf{M}$ are the net force and moment acting on the body, respectively, $\mathbf{I}$ is the moment of inertia tensor of the body, and $\boldsymbol{\omega}$ is the angular velocity of the body. The linear momentum equation, Eq. (3), is formulated in the global coordinate system, while the angular momentum equation, Eq. (4), is formulated in the body coordinate system with the origin at the body center of mass. The net force and moment acting on the body are evaluated on the body surface in discrete form by a midpoint method as:

$$\mathbf{F} = \sum_f \mathbf{t}_f A_f \tag{5}$$

$$\mathbf{M} = \sum_f \mathbf{r}_f \times (\mathbf{t}_f A_f) \tag{6}$$

where $\mathbf{t}_f$ is the traction vector (pressure and shear stress) acting on cell face f, A_f is the area of face f, and $\mathbf{r}_f$ is the distance vector between the body center of mass to the centroid of face f.

The overset mesh surrounding the embolus is a spherical shape of diameter 3.75, 3.75, and 4.7 mm, for each respective particle size. The thickness of the first mesh cell on the body is 15 μm for the 500 μm embolus case and 30 μm in the 1000 and 2000 μm embolus cases. The overset mesh size grows to about 120 μm at its outer edge. The mesh sizes at the overlap of the overset and background mesh should be of similar sizes for solution stability. For illustration, the overset mesh for the 500 μm embolus is shown in Fig. 2.

The 6DOF equations are integrated in time by a trapezoidal method. Implicit iterations are used between the 6DOF solver and the Eulerian flow solver to ensure stability and robustness. The time step size is also decreased to 0.1 ms for added stability. A typical maximum Courant number based on the embolus speed during systole is ≈ 0.5.

An appendix is included in this work showing several verification problems for the overset mesh technique as relevant to emboli transport. The test problems ensure that the sufficient spatial and temporal resolution are used herein.

Wall Collision Model

The overset method used here cannot resolve solid-on-solid contact between the 6DOF body and a wall. In order to prevent contact, the model applies a spring-like force when the distance between the body

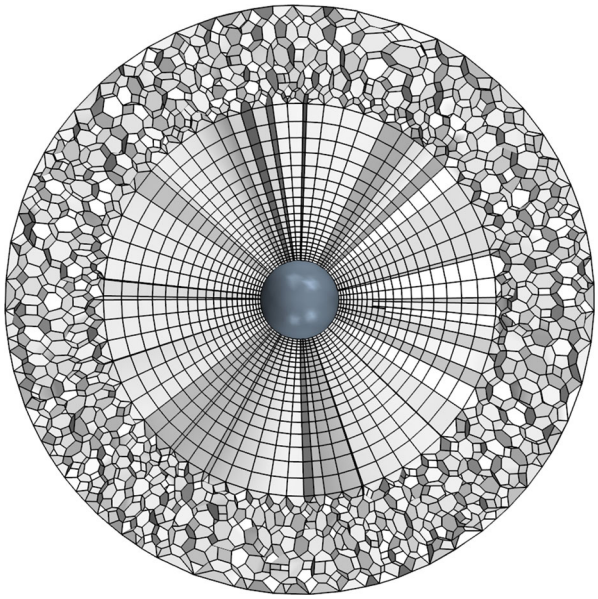

FIGURE 2. Cross-sectional view of the overset mesh surrounding the 500 μm embolus.

boundary and the lumen boundary is smaller that some cutoff range. The repulsive contact force, $\mathbf{f}_c$, is applied onto the 6DOF body mesh cell face in the direction normal to the corresponding lumen boundary face. The force is written as:

$$\mathbf{f}_c = k(x_0 - x)A_f\,\mathbf{n}_B \tag{7}$$

where k is an elastic coefficient, A_f is the body mesh cell face area, x is the distance between the face centroid and the opposing boundary, x_0 is the cutoff range, and $\mathbf{n}_B$ is the normal of the lumen boundary face adjacent to the body face. The total repulsive force on the body is the sum of all contributions from all faces on the body. In this work, a 250 μm cutoff range is used, and an elastic coefficient of 30 MPa/m is used. This was found to be sufficient to prevent overlap between the body surface and lumen surface while also maintaining solution stability. This value also ensures that the typical collision times are fast, $\lesssim$2 ms, compared to the flow time scale.

It should also be noted that the contact force can produce moments, and thus rotations, on the body. If the outward normals of a cell face on the embolus body and a cell face on the adjacent wall are not parallel during a collision event, then the contact force will produce a moment.

RESULTS

The proportions of the emboli traveling to the ICA are presented in Table 1 and shown graphically in Fig. 3. The total number of particle trajectories simulated are also shown in the table as the entry in parentheses. The trend shown in Fig. 3 and Table 1 agree with our hypothesis in two important aspects: (1) larger particles travel to the larger diameter ICA at a proportion greater than that of the Eulerian flow rate and (2) smaller particles act like nearly inertialess tracers particles. For reference, inertialess tracer particles are shown in Fig. 3a as zero diameter particles. Elaborating on point (1) above, the current trends are consistent with the previous results of Bushi *et al.*[7]

Elaborating on point (2) in the previous paragraph, the relative importance of the particle inertia can be quantified by the Stokes number. It is defined as the ratio of the particle response time to the flow time scale e.g., τ_p/τ_f where τ_p is the particle response time and τ_f is the flow time scale. Using the particle response time based on the Stokes drag, i.e., $\tau_p = \rho_p d^2/(18\,\mu)$, and a flow time scale based on the advective time in the CCA, i.e., $R/U \approx 0.02$ s, a particle of $\approx$ 1050 μm diameter has a Stokes number of 1.0. As the Stokes number $\to$ 0, a particle will act like an inertialess flow tracer.[12] A 500 μm embolus has a Stokes number $\approx$ 0.2 and thus only weak inertia; it has only about $\times$ 1.05 increased probability over the baseline of traveling to the ICA.

Importantly, the result confirms our hypothesis that the larger particle outcomes using a resolved model show quantitatively different results from those outcomes using a small particle model. For a 2000 μm embolus, the proportion of particles traveling to the ICA is 74.7 $\pm$ 1.3% (mean $\pm$ 95% confidence margin) for the small particle model, while it is 85.7 $\pm$ 5.4% for a resolved particle model. The two proportions calculated are in fact statistically different, $p < 0.05$, as determined by the Z-test for the difference between two proportions.

Videos of several resolved particle simulations are shown in the Supplementary Material.

DISCUSSION

This study did not discern meaningful differences at moderate-sized particles of 500 μm and 1000 μm which are 6.8 and 13.7% relative to the CCA diameter. However, statistical differences are found in the outcomes between the two modeling strategies for a 2000 μm embolus, which is a somewhat large particle at 27.3% relative to the CCA diameter. Therefore it is reasonable to conclude that *although qualitative trends remain the same, quantitative differences exist for simulations using a "small" vs. resolved particle approach beginning at size ratios greater than* 15–25%. Results for large-sized particles using "small" particle methods should be interpreted with caution.

TABLE 1. Descriptive statistics of particles.

	Particle diameter (μm)			
	0	500	1000	2000
Stokes number (–)	0.0	0.22	0.92	3.6
"Small" particle proportion	57.9 ± 1.2 (7007)	59.4 ± 1.2 (6181)	61.2 ± 1.2 (5893)	74.7 ± 1.3[a] (4291)
Resolved particle proportion	N/A	62.0 ± 8.8 (50)	62.0 ± 8.8 (50)	85.7 ± 5.4[a] (70)

The Stokes number is the ratio of the particle response time, $\rho_p d^2/(18\mu)$, to flow advective time scale, R/U. Proportions are the percentage of particles entering the ICA ± 95% confidence margin. Numbers in parentheses are the total number of particles simulated in each case. [a]Denotes proportions are statistically different at $p<0.05$ by the binomial test.

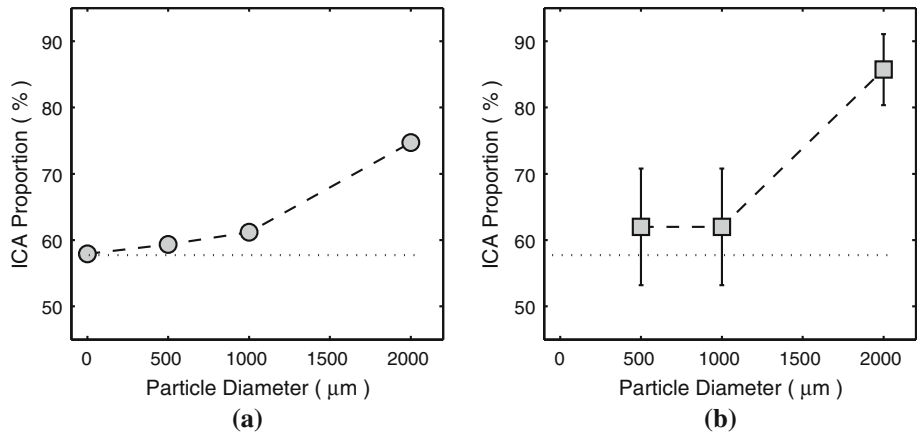

FIGURE 3. Proportions, in percent, of particles entering the ICA for (a) "small" particles and (b) resolved particles. Error bars are 95% CI in (b). Error bars are not shown in (a) due to small size. Dotted lines (...) show the Eulerian flow proportion to the ICA (57.7%).

This work also demonstrates the feasibility of extending the overset mesh framework to even larger emboli sizes or to non-spherical emboli. No modifications are required to the numerical framework to simulate non-spherical particles. The user must provide some additional inputs such as an appropriate mesh surrounding the rigid body and some of the body's properties, e.g., center of mass, principal moments of inertia. As an example, spheroidally-shaped emboli could be investigated in a further study. It reasonable to speculate that the trajectory of a spheroid would be affected by the rotation of the body. This is a fruitful area for future study which should be considered in future work.

This study provides further justification for a "small" particle approach using a modified Maxey–Riley equation for the motion. The small particle and resolved particle techniques give nearly identical results for emboli $\leq 1000\,\mu$m. This is in spite of the fact that several simplifying assumptions are made in the small particle model that are not inherent in the resolved particle model; for example, it is a one-way coupling method and the Basset history force is neglected.

It should be noted that the particle Reynolds numbers are not vanishingly small, and the finite Reynolds number corrections to the Maxey–Riley equation should be applied for moderately-sized emboli. The maximum Re_p was found to exceed 200 for 2000 μm emboli during systole. However, more typical values were found to be in the range of 5–100.

The neglect of the Basset history force may not be justified from physical considerations for emboli trajectory simulations. A scaling analysis of turbulent flows from Ling *et al.*[15] suggested that for nearly-neutrally-buoyant particles the history force is negligible when the square root of the Stokes number based on the smallest time scale of the flow is small. Surprisingly, however, the results here indicate that the emboli outcomes are not particularly sensitive to the history force despite the fact that the Stokes numbers, see Table 1, are not small. It is possible that the relevant time scale for assessing the history force should be the scale of unsteadiness in the background flow rather than the advective time. If that is the case, then the inverse of the cardiac cycle circular frequency, ≈ 0.1 s, is the relevant time scale. The Stokes numbers based on

the cardiac cycle time scale are 0.03, 0.1, and 0.5 for 500, 1000, and 2000 μm emboli, respectively. These Stokes numbers are sufficiently small, expect perhaps for the 2000 μm size, so that the neglect of the history force may be justified. Future work should investigate the relative strength of the history force for arterial flows.

The overset mesh approach does have a number of advantages to a small particle approach. First, the approach requires less modeling assumptions and should be considered of a higher physical fidelity. The functional forms of the various forces such as drag or history force, do not need to be specified *a priori*. Directly integrating the pressure and shear on the particle surface, e.g., Eqs. (5) and (6), is more fundamental than, for example, specifying a drag law. Second, the technique is inherently two-way coupled between the particle and Eulerian flow. No additional modeling assumptions are required to specify the transfer of momentum from the particle back to the Eulerian flow. Third, the technique resolves the particle rotation which may be important in the computation of spin-lift forces and wall collision forces.

On the other hand, the overset approach does have some drawbacks. This study found that a time step of $\times 2.5$ smaller and that $\times 2$ solver iterations are required to maintain stability and a well-converged result, a substantial penalty in terms of numerical cost. Furthermore, the interpolation between the background and overset mesh is not necessarily conservative as a finite volume method would be, especially with regards to conservation of mass. However, it was found here that mass errors were generally less than 0.1%, and were oftentimes even lower.

Given the increased computational costs of a resolved particle model using an overset mesh, it would be reasonable on practical considerations to use non-resolved particle models on some problems even for moderately-sized, $\gtrsim$ 20%, emboli. The current results show that a "small" particle model can produce correct trends and semi-quantitative results for moderate sizes. The two-way coupled particle simulations, such as those in Ref. 20, could be a good middle ground as they may able to extend the limit of applicability of "small" particle models but with less computational cost than a fully resolved model.

The sample size, particularly for the resolved particles, is deemed sufficient based on the fact that the sample is large enough such that the binomial distribution is in an asymptotic range and can be approximated as normal. A common rule for judging applicability of the normal approximation is if all possible binomial outcomes are less than three standard deviations away from the mean. This leads to a rule for a sample size n based on the the lower and upper limits of

$$n > 9\frac{1-p}{p} \quad \text{and} \quad n > \frac{p}{1-p} \tag{8}$$

where p is the binomial probability of a "successful" event. The rule gives $n > 12$ when the probability is 0.57 (the expected probability of a particle traveling to the ICA based on the mean Eulerian flow rate), $n > 27$ when the probability is 0.747 (the probability of a particle traveling to the ICA based on the "small" 2000 μm particle model), $n > 54$ when the probability is 0.857 (the probability of a particle traveling to the ICA based on the resolved 2000 μm particle model).

Although our results do not show detectable differences between the "small" and resolved models for 2000 and 1000 μm particles, it is possible that differences could be detected if the sample sizes are greatly increased. However, such differences may be so subtle that they are not of practical significance even if they may be statistically significant. Hypothetically, a probability of 61 vs. 62% predicted by a "small" or resolved model would not seem to be of practical significance. In such a case, it would still be reasonable to use a "small" particle model.

There are a number of limitations of this study. First, it is not known how generalizable the current results may be. This study examines a single segment of the vasculature, with a model based on the anatomy of a single subject. Previous work[8] has found that the proportions of emboli entering a vessel can vary significantly between patients. However, this will likely not change our conclusion that small and resolved particle simulations show quantitative differences at size ratios around 15–25%.

A second limitation is that the emboli entering the CCA are assumed to have a uniform spatial distribution across the vessel diameter. There are undoubtedly upstream flow effects which would preferentially steer emboli into a probability distribution that is spatially non-uniform. Nevertheless, whatever that distribution might be, it is not known *a priori*. However, the "small" and resolved particle initial conditions in this study sample the same probability distribution for their initial conditions. Therefore, any *relative* differences between the two cases can still be discerned by the current technique.

A third limitation is that gravity and buoyancy of emboli are not considered. However, it would seem unlikely for gravity to be the primary driver of emboli dynamics. Even for the largest particle size, the effective weight force, i.e., gravity force minus buoyancy force, is $\approx 2.0 \times 10^{-6}$ N. However, typical hydrodynamic forces are on the range of $10^{-5} - 10^{-4}$ N. The effective weight is

at least an order of magnitude smaller than hydrodynamic forces. This fact is also consistent with results of Carr[8] who found that re-orienting gravity to simulate a standing vs. a supine position did not appreciably change the distribution of particle trajectories. However, even if the effective weight force is small, gravitational effects may be important for emboli traveling over large distances or long transport times. Additionally, previous studies[4,10] have reported that gravitational forces were important in emboli trajectories. A sensitivity analysis should be performed in future work to more precisely quantify the effect of gravitational forces.

A fourth limitation is that the wall collision model is not identical between the "small" and resolved approaches. It is difficult to enable commensurate collision models in each case due to the aforementioned inability of the overset method to handle solid-on-solid contact. It cannot be ruled out that some of the differences in trajectories are due to the differences in collision models. However, the collision models are comparable to each other in two physically important respects. First, the collisions are fully elastic; no kinetic energy of a particle is dissipated during a collision event. Second, the collisions occur on a time scale fast relative to the flow time scale. The "small" particle collision model described in Section "Wall Collision Model" implicitly assumes the collision to be instantaneous. A typical collision time is calculated to be $\lesssim$2 ms for the resolved particle simulations. This time is much faster than the fluid advective time scale, $\approx$ 20 ms. When the collision times are fast, and thus effectively instantaneous, it is typically not necessary to resolve the specific nature of the collision. Instead, a coefficient of restitution, which is 1.0 for an elastic collision, is an effective lumped parameterization of the collision event.

In conclusion, this study shows the importance of using a resolved particle method for simulating the trajectory of large emboli in the vasculature in order to ensure physical fidelity of the trajectory. Based on the current results, a heuristic for determining the appropriateness of a resolved particle model is when the particle size ratio is $\geq$ 20%. Though a specific cutoff value could be refined based on more careful study of the problem, and a cutoff may depend on the particulars of a problem, the 20% cutoff is satisfactory for a first approximation.

APPENDIX: OVERSET VERIFICATION PROBLEMS

Three test problems for verification of the overset mesh are considered here to ensure that the sufficient spatial and temporal resolution are used for the emboli simulations. The three problems consider flows using an overset mesh with similar spatial resolution as the emboli results in Section "Results". The three test problems are: drag on a sphere in Stokes-Oseen flow; drag on a sphere near a solid wall in a low-Reynolds-number flow; settling of a sphere started from rest under gravity. This last case includes unsteady motion of a rigid body within the domain. In each case in the appendix, the same mesh is used as that for the 500 μm embolus results above to ensure similar levels of spatial scale are resolved.

Drag on a Stationary Sphere

The first verification problem calculates the steady drag sphere which is surrounded by an overset mesh. The background domain is a cylinder with a radius of 7.5 mm and height of 15 mm with the sphere located at its center. The background mesh is an unstructured polyhedral mesh with uniform nominal size of 0.2 mm. The flow is at a small, but not infinitesimal, Reynolds number. A uniform velocity is imposed at the front of the cylinder boundary, while an open boundary condition is applied at the cylinder sides and rear.

The computed drag is normalized by the Stokes drag, $6\pi\mu a U$, where a is the radius of the sphere and U is the freestream velocity. The drag is computed at three separate particle Reynolds numbers based on the particle diameter and freestream speed. The computed normalized drag is shown in Fig. 4 as a function of the sphere Reynolds number. The figure also shows the prediction from the Oseen correction to the Stokes drag and the Proudman and Pearson[21] correction to the Stokes drag. The normalized drag calculated with the overset method differed from the Proudman and Pearson expression by less than 0.5% for each case.

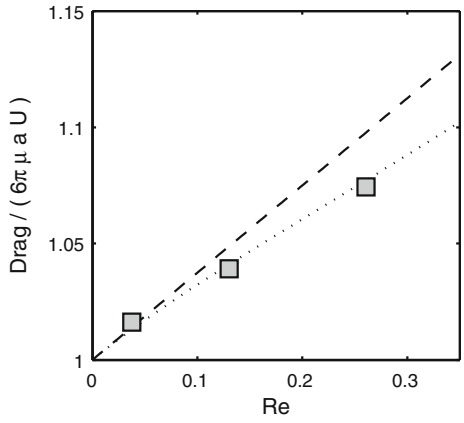

FIGURE 4. Normalized drag force on a sphere vs. Reynolds number based on the sphere diameter and freestream speed. Symbols are overset method, (dashed lines) Oseen drag (dotted lines) Proudman and Pearson drag.

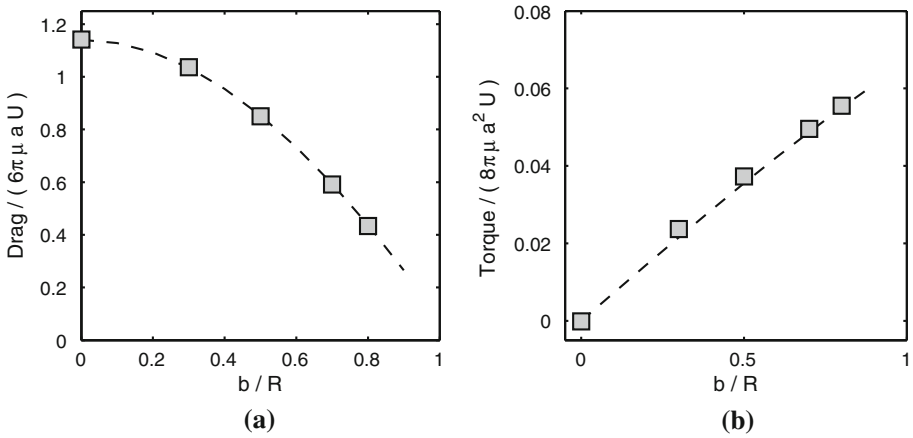

FIGURE 5. Dimensionless drag (a) and torque (b) on a sphere as a function of offset distance *b* normalized by the pipe radius *R*. Symbols are overset mesh results and (dashed lines) are the solutions from low Reynolds number theory.[13]

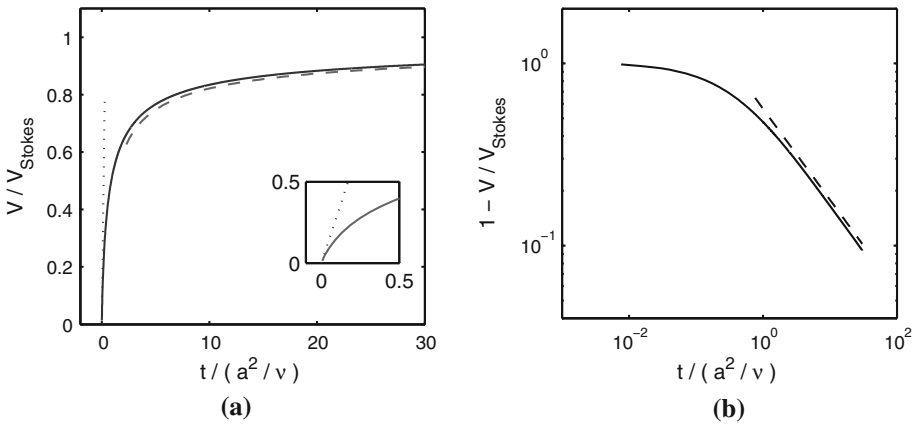

FIGURE 6. Unsteady velocity of sphere settling under gravity at low Reynolds number. a Shows velocity normalized by Stokes settling velocity vs. time normalized by the viscous diffusion time scale. Solid curve is the overset mesh result, (dotted lines) short-time asymptote solution, (dashed lines) long-time asymptote solution. Inset shows short-time behavior. b Log–log plot of relative differences of velocity to Stokes velocity. Solid curve is the overset mesh results, (dashed lines) long-time asymptote solution.

Drag and Torque on a Sphere Near a Wall

The second verification problem calculates the drag and torque on a stationary sphere as a function of distance from a wall. The surrounding domain is a cylindrical pipe of diameter 7.5 mm and length 25 mm. The background mesh is again an unstructured polyhedral mesh with uniform nominal size of 0.2 mm. The sphere is located in the center of the pipe along the axial direction, but can be offset from the pipe centerline by some distance b. The background flow in the pipe is a Poiseuille flow with a Reynolds number of 0.225 based on the pipe diameter. The drag in the streamwise direction is modified from Stokes drag by about 15% due to the small, but finite, size of the sphere. There is also a resulting torque in the azimuthal direction due to the velocity gradient over the sphere. The overset mesh results can be compared to solutions from low Reynolds number theory.[13] The drag and torque are plotted as a function of the offset distance for a single Reynolds number in Fig. 5.

The predicted dimensionless drag differs from the theoretical drag by less than 0.5% in all cases. The differences for the dimensionless torque are $\lesssim 10\%$. However, the magnitude of the dimensional torque is $\sim 10^{-14}$ N m. So the code may only be able to resolve the torque to two significant figures due to the machine roundoff.

Sphere Settling Under Gravity

The last verification problem investigates the unsteady motion of a sphere settling under the influence of gravity as it approaches terminal speed. The sphere

is released from rest in an initially quiescent fluid. The overset mesh surrounding the sphere is allowed to translate as the body falls due to gravitational settling. The speed and displacement of the body are solved as a function of time. The computed velocity can be compared to analytical results for a short-time asymptote and long-time asymptote of the Maxey–Riley equation.[24]

The fluid domain is a circular cylinder of radius 7.5 mm and height 15 mm. The time step size is 0.1 ms. The density ratio of the sphere to fluid is $\approx$ 1.05 which is the same as that used in the embolus simulations. The terminal Stokes settling velocity, V_{Stokes}, is 0.68 mm/s. The Reynolds number based on the Stokes velocity and sphere diameter is 0.036.

The results of the settling simulation by overset technique are shown graphically in Fig. 6. Excellent agreement is found with the overset method and the analytical solutions. At short times, the dominant forces on the sphere are buoyancy/weight and added mass. The short solution shows free fall-like behavior, $v \sim t$. At long times, the dominant forces on the sphere are buoyancy/weight, quasi-steady drag, and Basset history force. Because of the kernel function in the Basset force, the sphere approaches terminal speed $\sim t^{-1/2}$. The dashed line in Fig. 6b shows the asymptotic solution exhibiting $t^{-1/2}$ decay, and the overset solution shows the correspondingly correct asymptotic behavior.

ELECTRONIC SUPPLEMENTARY MATERIAL

The online version of this article (doi:https://doi.org/10.1007/s13239-019-00430-5) contains supplementary material, which is available to authorized users.

ACKNOWLEDGMENTS

Thanks to Bradley Davidson, Kristian Debus, and Ehsan Rajabi for helpful comments during the preparation of the manuscript.

CONFLICT OF INTEREST

P. M. McGah is an employee of Siemens PLM Software Inc., the company that produces and sells Simcenter STAR-CCM+.

HUMAN SUBJECTS AND ANIMAL SUBJECTS ETHICAL STATEMENT

No animal studies were conducted by the author for this article. No human studies were conducted by the author for this article.

REFERENCES

[1]Abolfazli, E., N. Fatouraee, and B. Vahidi. Dynamics of motion of a clot through an arterial bifurcation: a finite element analysis. *Fluid Dyn. Res.* 46(5):055505, 2014.
[2]Aliseda, A., V. K. Chivukula, P. M. Mcgah, A. R. Prisco, J. A. Beckman, G. J. Garcia, N. A. Mokadam, and C. Mahr. LVAD outflow graft angle and thrombosis risk. *ASAIO J.* 63(1):14–23, 2017.
[3]Arboix, A., and J. Alioc. Cardioembolic stroke: clinical features, specific cardiac disorders and prognosis. *Curr. Cardiol. Rev.* 6(3):150–161, 2010.
[4]Aycock, K. I., R. L. Campbell, K. B. Manning, and B. A. Craven. A resolved two-way coupled CFD/6-DOF approach for predicting embolus transport and the embolus-trapping efficiency of IVC filters. *Biomech. Model. Mechanobiol.* 16(3):851–869, 2017.
[5]Barbut, D., F. S. F. Yao, Y. W. Lo, R. Silverman, D. N. Hager, R. R. Trifiletti, and J.P. Gold. Determination of size of aortic emboli and embolic load during coronary artery bypass grafting. *Ann. Thorac. Surg.* 63(5):1262–1265, 1997.
[6]Benjamin, E. J., S. S. Virani, C. W. Callaway, A. M. Chamberlain, A. R. Chang, S. Cheng, S. E. Chiuve, M. Cushman, F. N. Delling, and R. Deo, et al. Heart disease and stroke statistics 2018 update: a report from the American Heart Association. *Circulation* 137(12):e67–e492, 2018.
[7]Bushi, D., Y. Grad, S. Einav, O. Yodfat, B. Nishri, and D. Tanne. Hemodynamic evaluation of embolic trajectory in an arterial bifurcation: an in-vitro experimental model. *Stroke* 36(12):2696–2700, 2005.
[8]Carr, I. A., N. Nemoto, R. S. Schwartz, S. C. Shadden. Size-dependent predilections of cardiogenic embolic transport. *Am. J. Physiol. Heart Circ. Physiol.* 305(5):H732, 2013.
[9]Chung, E. M., J. P. Hague, M. A. Chanrion, K. V. Ramnarine, E. Katsogridakis, and D. H. Evans. Embolus trajectory through a physical replica of the major cerebral arteries. *Stroke* 41(4):647–652, 2010.
[10]Fabbri, D., Q. Long, S. Das, M. Pinelli. Computational modelling of emboli travel trajectories in cerebral arteries: influence of microembolic particle size and density. *Biomech. Model. Mechanobiol.* 13(2):289–302, 2014.
[11]Hadžić, H. Development and application of finite volume method for the computation of flows around moving bodies on unstructured, overlapping grids. Ph.D. thesis, Technische Universität Hamburg, 2006.
[12]Haller, G. and T. Sapsis. Where do inertial particles go in fluid flows? *Physica D* 237(5):573–583, 2008.

[13]Happel, J. and H. Brenner. Low Reynolds Number Hydrodynamics: With Special Applications to Particulate Media. New York: Springer, 1981.
[14]Holdsworth, D., C. Norley, R. Frayne, D. Steinman, and B. Rutt. Characterization of common carotid artery blood-flow waveforms in normal human subjects. *Physiol. Meas.* 20(3):219, 1999.
[15]Ling, Y., M. Parmar, and S. Balachandar. A scaling analysis of added-mass and history forces and their coupling in dispersed multiphase flows. *Int. J. Multiph. Flow* 57:102–114, 2013.
[16]Manning, W. J., R. M. Weintraub, C. A. Waksmonski, J. M. Haering, P. S. Rooney, A. D. Maslow, R. G. Johnson, and P.S. Douglas. Accuracy of transesophageal echocardiography for identifying left atrial thrombi: a prospective, intraoperative study. *Ann. Intern. Med.* 123(11):817–822, 1995.
[17]Maxey, M. R. and J. J. Riley. Equation of motion for a small rigid sphere in a nonuniform flow. *Phys. Fluids* 26(4):883–889, 1983.
[18]Mei, R. Velocity fidelity of flow tracer particles. *Exp. Fluids* 22(1):1–13, 1996.
[19]Mukherjee, D., N. D. Jani, K. Selvaganesan, C. L. Weng, and S. C. Shadden. Computational assessment of the relation between embolism source and embolus distribution to the circle of willis for improved understanding of stroke etiology. *J. Biomech. Eng.* 138(8):081008, 2016.
[20]Mukherjee, D., J. Padilla, S. C. Shadden. Numerical investigation of fluid–particle interactions for embolic stroke. *Theor. Comput. Fluid Dyn.* 30(1–2):23–39, 2016.
[21]Proudman, I. and J. R. A. Pearson. Expansions at small Reynolds numbers for the flow past a sphere and a circular cylinder. *J. Fluid Mech.* 2(3):237–262, 1957.
[22]Reichenspurner, H., J. A. Navia, G. Berry, R. C. Robbins, D. Barbut, J. P. Gold, and B. Reichart. Particulate emboli capture by an intra-aortic filter device during cardiac surgery. *J. Thorac. Cardiovasc. Surg.* 119(2);233–241, 2000.
[23]Swaminathan, T. N., H. H. Hu, and A. A. Patel. Numerical analysis of the hemodynamics and embolus capture of a Greenfield vena cava filter. *J. Biomech. Eng.* 128(3):360–370, 2006.
[24]Temkin, S. Suspension Acoustics: An Introduction to the Physics of Suspensions. Cambridge: Cambridge University Press, 2005.
[25]Van Hinsberg, M. A. T., J. H. M. ten Thije Boonkkamp, and H. J. H. Clercx. An efficient, second order method for the approximation of the Basset history force. *J. Comput. Phys.* 230(4):1465–1478, 2011.
[26]Westerhof, N., J. W. Lankhaar, and B. E. Westerhof. The arterial Windkessel. *Med. Biol. Eng. Comput.* 47(2):131–141, 2009.
[27]Zierler, R. E., D. F. Leotta, K. Sansom, A. Aliseda, M. D. Anderson, and F. H. Sheehan. Development of a duplex ultrasound simulator and preliminary validation of velocity measurements in carotid artery models. *Vasc. Endovasc. Surg.* 50(5):309–316, 2016.

Publisher's Note Springer Nature remains neutral with regard to jurisdictional claims in published maps and institutional affiliations.